

Original Article

# Unsupervised Lumbar IVD Localization and Segmentation using GFMM and Boundary Refined Region Growing Techniques

S. Shirly<sup>1</sup>, R. Golden Nancy<sup>2</sup>, R. Venkatesan<sup>3</sup>, T. Jemima Jebaseeli<sup>4</sup>, K. Ramalakshmi<sup>5</sup>

<sup>1,2,3,4</sup>Department of Computer Science and Engineering, Karunya Institute of Technology and Sciences, Coimbatore, Tamilnadu, India.

<sup>5</sup>Department of Computer Science and Engineering, Alliance University, Bangalore, India.

Received: 23 February 2022

Revised: 08 April 2022

Accepted: 11 April 2022

Published: 26 April 2022

**Abstract** - Low Back Pain is caused because of Lumbar Intervertebral Disc (IVD) degeneration, and it is one of the most suffered problems by a large population. In this paper, the lumbar IVD is automatically localized and segmented using Gabor Filter with Mathematical Morphology and novel Boundary Refined Region Growing techniques, respectively. An MRI dataset is used to validate the suggested approach, consisting of 180 IVDs from 30 subjects. Initially, the Gabor Filter with Mathematical Morphology and Support Vector Machine with Local Binary Pattern techniques are used in localizing the lumbar IVD. In comparison to performance, Gabor Filter with Mathematical Morphology localized with 100% accuracy. In contrast, SVM localized with 89.4% for the precision range of 2mm. The Gabor Filter with Mathematical Morphology attained an accuracy of 96.9% for the 0.6mm precision range, which is comparatively higher than the accuracy of SVM for the 2mm precision range. Then the segmentation is preceded by the novel Boundary Refined Region Growing technique on the lumbar IVD image localized by Gabor Filter with Mathematical Morphology, achieving a better Dice Similarity Index, sensitivity, and specificity of 86.2%, 92%, and 99%, respectively.

**Keywords** - Lumbar Intervertebral Disc, Magnetic Resonance Imaging, Gabor filter, Mathematical Morphology, Support vector machine, Boundary refined region growing.

## 1. Introduction

The intervertebral disc is a fibrocartilage structure found between the two vertebrae of the spine. It comprises a nucleus pulposus surrounded by an annulus fibrosus layer. The nucleus pulposus is normally adequately hydrated and functions as a stress absorber. The nucleus pulposus loses its capacity to stay hydrated and stiffens due to many circumstances such as trauma, age, hereditary variables, and stress [1]. Lumbar IVD disc degeneration can cause low back discomfort and is the cause of major surgical spine surgeries [2].

MRI is one of the most preferred and sophisticated modalities for diagnosing disc degeneration in clinical practice. As most of the degeneration occurs near the marrow of the spine, the mid-sagittal slice is the frequently used view for finding disc degeneration in MRI. Radiologists may see the discs' nucleus pulposus and annulus fibrosis in the sagittal image [3]. In the sagittal view of a normal disc, the nucleus pulposus shows as a brilliant ellipse, whereas the annulus fibrosis appears as a black ring surrounding the nucleus pulposus. Alternatively, the degenerated IVD appears darker. The nucleus pulposus cannot be correctly differentiated from the annulus fibrosis, and the shape of the degenerated disc will be partly irregular [4].

Normally, the radiologists manually do the localization and segmentation in MRI. The result of this manual delineation process is based on the knowledge and experience of the radiologists. Manual localization and segmentation are more tedious and time-consuming; therefore, a reliable computer-aided diagnostic technique for automatic localization and segmentation of lumbar IVD would be very useful and time-saving. It is a difficult problem because of the wide range of variations in discs and vertebrae's form, number, size, and appearance.

Many types of research on the localization and segmentation of IVDs have been conducted in recent years. Schmidt, Kappes [5] proposed a probabilistic inference method to measure the location of the IVD in MRI, but it fails to localize in case of any fracture. Zhu, He [6] proposed a Gabor filter bank and adaptive thresholding technique to localize and segment the lumbar IVD, and the limitation is that the accuracy of the curvature of the spine should be improved to diagnose the disease. Chevrefils and Cheriet [7] used a watershed and morphological method to extract the spinal canal and IVD from M.R. images of scoliotic individuals. The major drawback was over-segmentation, and it needs manual intervention for localization. Oktay and Akgul [8] created a Markov Random Field (MRF) based on a Support Vector Machine



(SVM) to localize the lumbar IVD. Still, the accuracy can be improved. Michopoulou, Costaridou [4] proposed a semi-automatic approach, namely Atlas-Fuzzy C-Means (FCM), Atlas-Robust FCM (RFCM), and Elastic Atlas-RFCM to segment the IVD. Still, the major disadvantage of these techniques is the need for large data training and rigid manual registration. Raja, Corso [9] employed a two-level probabilistic model; Peng, Zhong [10] proposed a model-based searching method for localizing the spine discs, but both approaches require manual intervention. In IVD segmentation-related literature, Hough transform, and self-adaptive window [11], FCM and active counter model [2], anisotropic-oriented flux model [12], and discrete simplex surface model [13] have been proposed to segment the lumbar IVDs effectively but these techniques also require manual assistance. The primary goal of this work is to provide a strategy for lumbar IVD localization and segmentation that does not require any manual intervention.

Most of the researchers used the Gabor filter (unsupervised) [6, 13-16] and SVM (supervised) [8, 17, 18] for localization as it gives better results. In this study, the lumbar IVD is automatically localized using GFMM and SVM with Local Binary Pattern (LBP) techniques. Then the results are compared and quantitatively evaluated to find the best localization technique. On the better

accurate localized lumbar IVD image, the segmentation will be preceded by a novel boundary refined region growing technique.

## 2. Dataset

The dataset contains the T2-weighted lumbar spine M.R. image for 30 subjects collected from the Rio scan centre, Tirunelveli. Images were acquired using the Siemens MAGNETOM Avanto 1.5 T MRI scanner with the following acquisition parameters: fast spin-echo imaging sequence, slice thickness = 5 mm, slice spacing = 0.5 mm, resolution =  $448 \times 448$ . The centre of the IVDs and the IVDs of each lumbar M.R. image were manually delineated by a physician. The sagittal view of the lumbar M.R. image consists of five vertebrae and six lumbar intervertebral discs [8]. There is a total of  $30 \times 5 = 150$  lumbar vertebrae and  $30 \times 6 = 180$  lumbar IVDs. Of 180 lumbar IVDs, 81 lumbar IVDs have pathologies, and 99 lumbar IVDs are pathology free. The localization and segmentation of the lumbar IVD using the proposed methods are simulated in MATLAB2017b.

## 3. Methodology

Fig. 1 shows the experimental flow, and the major functionalities carried out in the segmentation process of the lumbar MRI.

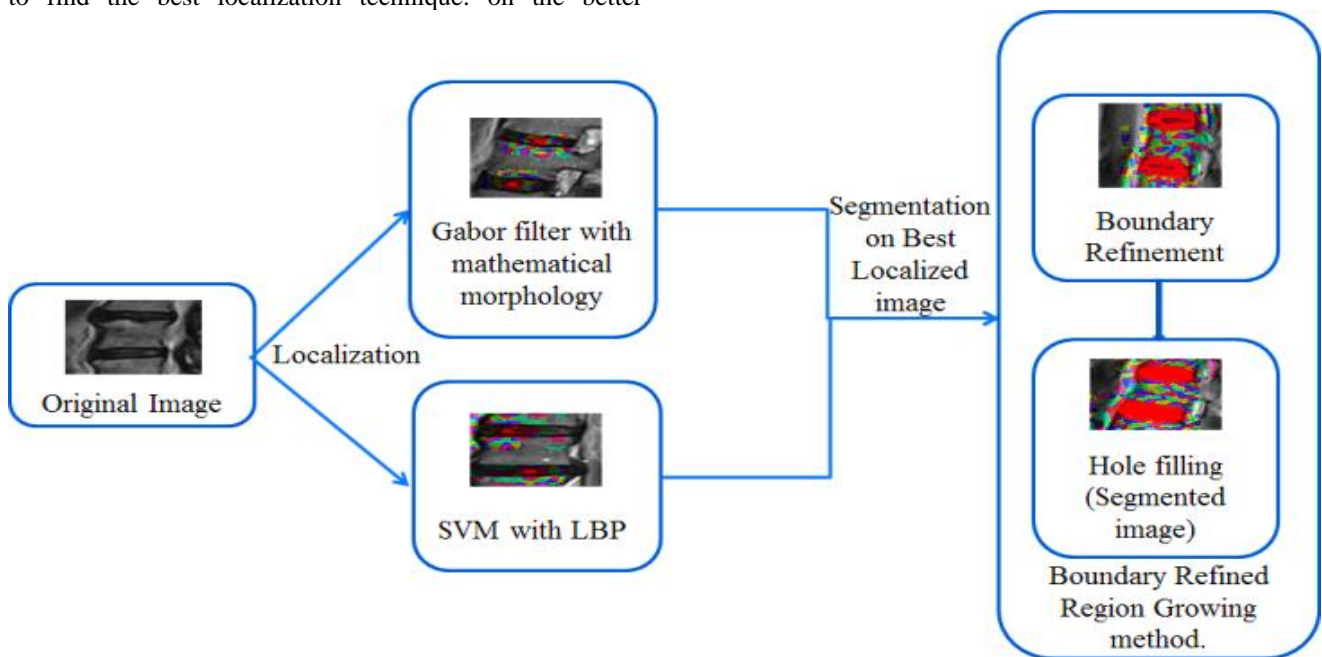


Fig. 1 Flow Diagram of Localization and Segmentation of Lumbar IVDs.

### 3.1 Localization of Lumbar IVDs

To acquire the exact location of the IVD, the localization of IVD is used, and it is done using two techniques, namely GFMM and SVM with LBP. In the GFMM technique, the Gabor filter technique transforms and projects the edges and boundaries of the lumbar vertebrae of the given MRI. Then mathematical morphological technique, namely erosion based on horizontal-wise maximum response extraction, is applied to the resultant image of the Gabor filter, and it erodes the

unwanted edges and boundaries, followed by a dilation process on the eroded image dilates the edges and boundaries. From this, the midpoint of the lumbar IVD is automatically localized. In SVM-based localization, the features are extracted using LBP, and those features are used by SVM to localize the lumbar IVD.

### 3.2 Gabor Filter with Mathematical Morphology (GFMM)

Dennis Gabor developed the Gabor filter, an extension of the gaussian-window Fourier transform. [19]. It is widely used for image process application that highlights the edges and boundaries by improving the resolution. the Gabor filter is defined as [20].

$$(a, b, \theta_\mu, w_v) = \frac{1}{2\pi\sigma_a\sigma_b} \exp \left\{ -\frac{1}{2} \left[ \left( \frac{a'}{\sigma_a} \right)^2 + \left( \frac{b'}{\sigma_b} \right)^2 \right] \right\} + iw_v a' \quad (1)$$

Where  $a' = a \cos \theta_\mu + b \sin \theta_\mu$ ,  $b' = -a \sin \theta_\mu + b \cos \theta_\mu$  are the spatial locations of pixels, the parameter  $\sigma$  of the Gabor function is different in 'a' (horizontal) and 'b' (vertical) directions and the parameters  $\sigma$ ,  $\theta_\mu$ , and  $w_e$  represent the Gaussian window, direction, and wavelength of the Gabor filter [6]. It has K scales varying from 1 to 5 and S directions varying from  $0^\circ$  to  $360^\circ$  at  $45^\circ$  to describe the local image features [21]. It can be set with different scales, frequencies, and directions to get a series of Gabor images.

### 3.3 Pseudo Code for Localization using GFMM Technique

Input: Lumbar Spine MR Image (Given MRI).  
 Step 1: Gabor filter is applied to the given MRI.  
 $Lumbar_{gf} \leftarrow G.F.(\theta, S, F)(Lumbar_{img})$   
 Step 2: the output of the Gabor filter is converted into a binary image using the Otsu threshold method.  
 $Lumbar_{Bimg} \leftarrow Otsu(Lumbar_{gf})$   
 Step 3: Erosion is applied to the binary image with varying length (l) and degree (d), and the eroded images are combined to get the maximum horizontal response eroded image.  
 $HM_{axR} \leftarrow \text{erode}_{(l,d)}(Lumbar_{Bimg}) \mid \text{erode}_{(l,d)}(Lumbar_{Bimg}) \mid \text{erode}_{(l,d)}(Lumbar_{Bimg})$   
 Step 4: Dilation is applied on the  $HM_{axR}$ .  
 $Dilation_{img} \leftarrow \text{dilate}_{(disk,r)}(HM_{axR})$   
 Step 5: the unwanted connected components are removed, and the final IVD mask is set on the  $Lumbar_{img}$ .  
 $IVD_{Boundary} \leftarrow \text{ConnectedComponents}_{(>minthresholdpixel.<maxthreshold pixel)}(Dilation_{img})$   
 Output: the final IVD mask image.

In the proposed method, the given lumbar image ( $Lumbar_{img}$ ) (Fig. 2 (a)) is fed into the Gabor filter with the setting of various directions, scales, and frequencies to generate a set of Gabor images. the exact Gabor picture is derived from these Gabor images based on experience by setting theta as  $180^\circ$ , frequency as 0.2, and scale as 5 ( $Lumbar_{gf}$ ) (Fig. 2 (b)) is obtained. Fig. 2(b) is a Gabor response image highlighting the vertebral and IVD boundaries. Then the  $Lumbar_{gf}$  is converted into a binary image ( $Lumbar_{Bimg}$ ) using the Otsu threshold method, and the result is shown in Fig. 2. A comparison of Fig. 2(b) and 2(c) reveals that Fig. 2(b) depicts the vertebral and IVD borders more clearly.

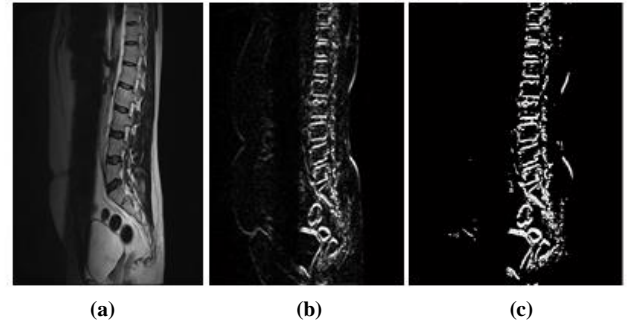


Fig. 2 (a) Given MRI ( $Lumbar_{img}$ ). (b) Gabor Response for given MRI ( $Lumbar_{gf}$ ). (c) Binary Version of Gabor Response ( $Lumbar_{Bimg}$ ).

### 3.4 Mathematical Morphology

Erosion is a morphological transformation that combines the two set elements (different image dimensions) using vector subtraction. It is also known as the shrinking of the original image. If X and Y are set in N-space Euclidean ( $E^N$ ) with elements  $a = (a_1, \dots, a_N)$  and  $b = (b_1, \dots, b_N)$  respectively. the set of all elements for which  $a + b \in X$  for any  $b \in Y$  is the erosion of X by Y. the erosion of X by Y is represented as  $X \ominus Y$  and is defined as,

$$X \ominus Y = \{a \in E^N \mid a + b \in X \text{ for every } b \in Y\} \quad (2)$$

In the proposed method, the line filter is selected as the structuring element for the erosion of the  $Lumbar_{Bimg}$  to get the IVD boundaries. the expected outcome of the  $Lumbar_{Bimg}$  is to get the pathological IVD boundaries in labelling order as T12-L1 to L5-S1. Still, the IVD boundaries are not in order while doing erosion in the  $Lumbar_{Bimg}$ . To overcome this issue, horizontal-wise maximum response extraction is used. in horizontal-wise maximum response extraction, the  $Lumbar_{Bimg}$  is rotated in an anti-clockwise direction of  $90^\circ$  and then the erosion with line filter structuring element along with length and degree set as (15,0), (15,15), and (45,0) according to the experience to erode the unwanted white spots and extract the IVD boundaries in order and the resultant images are combined to get horizontal-wise maximum response eroded image ( $HM_{axR}$ ) as shown in Fig. 3(a).

Dilation is a morphological dual of erosion, and it is also a morphological transformation that combines the two set elements using vector addition; it expands the input image. If X and Y are set in  $E^N$  with elements  $x = (x_1, \dots, x_N)$  and  $y = (y_1, \dots, y_N)$  respectively, then the dilation of X by Y is the set of all sum of the possible pairing elements. It can be denoted as  $X \oplus Y$ , and it can be defined as [22].

$$X \oplus Y = \{z \in E^N \mid z = x + y \text{ for some } x \in X \text{ and } y \in Y\} \quad (3)$$

The dilation approach is employed to expand as  $HM_{axR}$  by setting the structuring element as disk and the radius as 2mm. Fig. 3(b) depicts the result of the dilation image. the pixel value below 100 and above 580 are set to remove the white spots other than the IVD boundaries. Then, the centre point of the lower and upper boundaries

are detected from the valid upper and lower boundary connected components of the lumbar IVD. From this, the midpoint for localization is estimated. Fig. 3(a) shows the boundaries of the IVDs, and Fig. 3(b) shows the expanded boundaries of IVDs. the final IVD boundary mask is set on the Lumbar<sub>img</sub> as shown in Fig. 3(c), and the localized IVD is shown in Fig. 3(d).

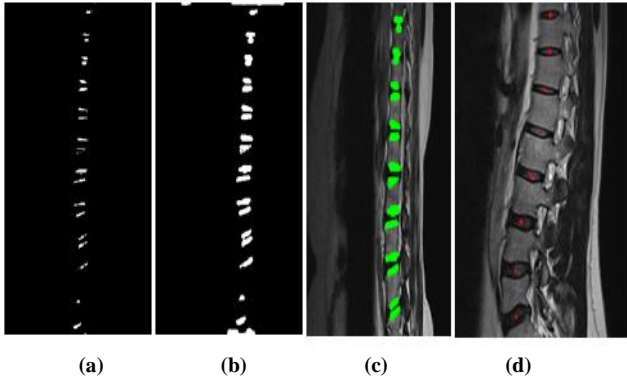


Fig. 3 (a) Combined Erosion (HM<sub>axR</sub>). (b) Dilation (Dilation<sub>img</sub>). (c) IVD Boundary Mask. (d) Localized IVD.

### 3.5 Support Vector Machine with Local Binary Pattern (SVM with LBP)

The SVM with LBP technique is used for the localization of lumbar IVD. LBP illustrates the shape and texture of an image; the features are extracted by dividing the images into several small regions. the features include binary patterns, which illustrate the pixels surrounding the regions. the obtained features are concatenated into a single feature histogram, which summarises the representation of the image, and the images may be compared by assessing histogram similarity. It is defined as a binary pixel intensity comparison between the centre and surrounding pixel [23].

$$LBP(x_n, y_n) = \sum_{s=0}^7 K(l_s - l_n)2^s \quad (4)$$

Where  $(x_n, y_n)$  is the given pixel position,  $l_n$  denotes the grey value of the centre pixel, and  $l_s$  denote the grey values of the surrounding pixel. LBP extracts the features of the lumbar M.R. image, and the LBP histogram is shown in Fig. 4. in SVM [24], among the 180 IVDs, 120 IVDs (20 subjects) are used to train the SVM model, and 60 IVDs (10 subjects) are used to test and validate the models. the extracted feature is used in SVM for localizing the lumbar IVD.

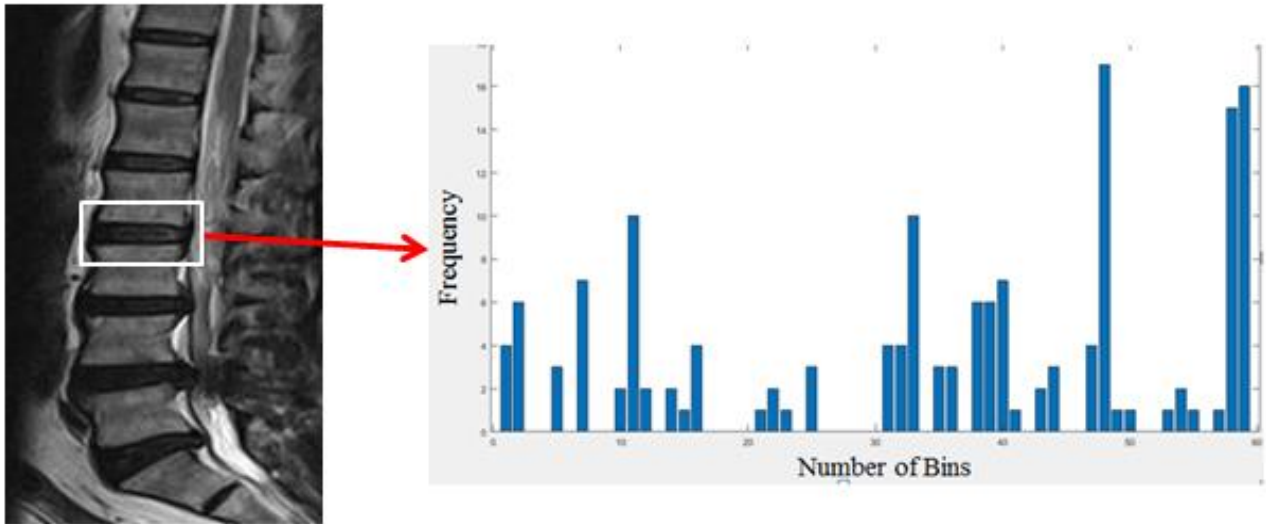


Fig. 4 LBP Histogram for L1-L2 IVD

Performance-based comparison on localization reveals that GFMM based localization localizes the IVD with the accuracy of 96.9% and 100% for the 0.6mm and 2mm precision range, respectively. in contrast, SVM-based localization gives an accuracy of 89.4% for the 2mm precision range, but with a 0.6mm precision range, SVM could not localize most of the IVDs, as shown in Table 1. the other advantage of the Gabor filter is that it is an unsupervised and fully automatic technique, but SVM is a supervised technique. So, comparatively GFMM based localization is better than SVM-based localization.

Therefore, the segmentation is preceded by the images localized by the GFMM technique.

Table 1. Overall Localization Accuracy using Gabor Filter and SVM

Localization Method	P <sub>n</sub> (%)	
	n = 2mm	n = 0.6mm
GFMM	100%	96.9%
SVM with LBP	89.4%	Most of the IVDs are not localized.

### 3.6 Segmentation using Boundary Refined Region Growing Technique

#### 3.6.1 Pseudo Code for Segmentation using Boundary Refined Region Growing Technique

Input: Localized IVD.

Step 1: the closest black pixel (less than 35) is randomly selected from one connected component.

$$I_{\text{pixel}} \leftarrow \text{IVD}_{\text{Boundary}} \text{ (less than 35)}$$

Step 2: the neighbouring pixels of the initial pixel is added to the selected pixel until it is needed.

$$AF_{\text{Boundary}} \leftarrow I_{\text{pixel}} \text{ (Neighbouring Fetch)}$$

Step 3: Step 2 is repeated until all the pixels with a value less than 35 are grouped.

Step 4: the hole filing method is used in filling the hole as in filling the inner layer.

$$IVD_{\text{Seg}} \leftarrow AF_{\text{Boundary}} \text{ (Hole Filling)}$$

Output: Segment the lumbar image.

The basic idea of the boundary refined region growing technique is to collect pixels with similar values to form a boundary. the lumbar intervertebral disk consists of annulus fibrosis and nucleus purposes. in this, the annulus fibrosis is closest to black and the nucleus purposes in grey colour in the MRI image. in the proposed method, the annulus fibrosis (closest to black) is marked using the boundary refinement method by selecting an initial pixel (less than 35) from the connected component. the initially selected pixel attempts to fetch the neighbouring pixels to refine the boundary. This step is repeated until the boundary refinement is done and the annulus fibrosis is marked, as shown in Fig. 5(a). Then the nucleus purposes are filled using the hole filling method, and the result is shown in Fig. 6.

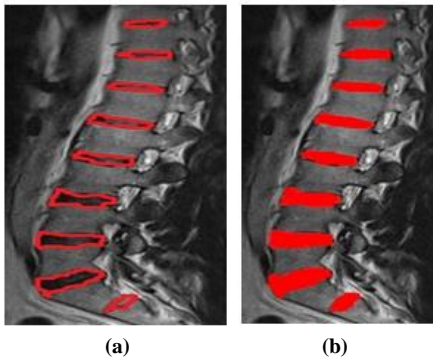


Fig. 5 (a) Boundary refined annulus fibrosis. (b) Segmented lumbar IVDs

## 4. Experimental Results and Analysis

### 4.1 Validation Framework

To evaluate the accuracy of the localization process, statistical error analysis, namely Mean Localization Distance with Standard Deviation and Successful Localization Rate, were calculated for the simulated results.

### 4.2 Mean Localization Distance with Standard Deviation

The localization distance D for each IVD centre was computed using equation (5).

$$D = \sqrt{(\Delta x)^2 + (\Delta y)^2} \quad (5)$$

Where  $\Delta x$  and  $\Delta y$  are respectively x, y coordinates the variation between the ground truth and the automatically localized IVD. the least D value denotes the localization with better accuracy; the lower the mean value, the higher the accuracy rate. the SD indicates the closeness of the derived value with the expected value. Mean localization distance and standard deviation are defined as follows:

$$\text{Mean Localization Distance (MLD)} = \frac{\sum_{i=1}^{T_{img}} \sum_{j=1}^{T_{IVD}} D_{ij}}{T_{img} T_{IVD}} \quad (6)$$

Standard Deviation (SD) =

$$\sqrt{\frac{\sum_{i=1}^{T_{img}} \sum_{j=1}^{T_{IVD}} (D_{ij} - \text{Mean localization distance})^2}{T_{img} T_{IVD}}} \quad (7)$$

Time is the total number of M.R. images, and  $T_{IVD}$  is the total number of IVDs.

### 4.3 Successful Localization Rate (SLR)

If the distance between the ground truth centre and the automatically localized IVD centre is less than n mm, then the localization of IVD is successful. the successful localization rate  $P_n$  is defined as follows:

$$P_n = \frac{\text{Total No. of IVD Localization}}{\text{Total No. of IVDs}} \times 100\% \quad (8)$$

### 4.4 Performance Analysis of GFMM Based Localization

The performance of the GFMM localization technique is quantitatively measured using the MLD, SD, and SLR. for the precision range  $n=0.6\text{mm}$ , the calculated MLD ranged between 0.003mm to 0.544mm, and S.D. ranged between 0.015mm to 0.305mm, respectively. the overall respective mean value of MLD and SD are 0.205mm and 0.152mm. the SLR is also calculated, and it gives 96.9% accuracy. for the precision range of  $n=2\text{mm}$ , the calculated MLD ranged between 0.138mm to 1.09mm, and S.D. ranged between 0.001mm to 0.745mm. the overall mean value of MLD and SD is 0.473mm and 0.373mm, and the SLR gives 100% accuracy.

### 4.5 Performance Analysis of SVM Based Localization

The performance of SVM with the LBP localization technique is quantitatively measured using the above said two metrics. for the precision range of  $n=2\text{mm}$ , the MLD ranged between 0.150mm to 2.936mm, and S.D. ranged between 0.092mm to 0.960mm. the overall mean value for MLD and SD is 1.006mm and 0.491mm, and the SLR is 89.4%. SVM-based localization does not give better accuracy for the 0.6mm precision range.

### 4.6 Comparison of GFMM and SVM Localization

Fig. 6 and 7 shows the comparison of MLD and S.D. of lumbar IVD localization by GFMM ( $n = 0.6\text{mm}$ ) and SVM with LBP ( $n=2\text{mm}$ ). Fig. 8 and 9 compare the MLD and S.D. of lumbar IVD localization by GFMM ( $n=2\text{mm}$ ) and SVM with LBP ( $n = 2\text{mm}$ ). It is observed that the

GFMM MLD (n = 0.6mm, 2mm) has the lowest value of 0.003mm and 0.138mm respectively, and SVM MLD (n = 2mm) has the lowest value of 0.150mm. Likewise, the GFMM SD (n = 0.6mm, 2mm) have the lowest value of 0.015mm and 0.003mm, respectively, and SVM SD (n = 2mm) has the lowest value of 0.092m and which shows that the GFMM technique with the precision range 0.6mm and 2mm and SVM with LBP (n = 2mm) gives better

accuracy. Table 1 shows the overall successful localization rate ( $P_n$ ) of the GFMM technique for precision range (n = 0.6mm, 2mm) and SVM with LBP (n = 2mm); it shows that the GFMM accuracy rate is higher with 96.9% for 0.6mm precision range and 100% for 2mm precision range than the SVM with LBP. So, comparatively, the GFMM technique is better than the SVM with LBP for localization of lumbar IVD.

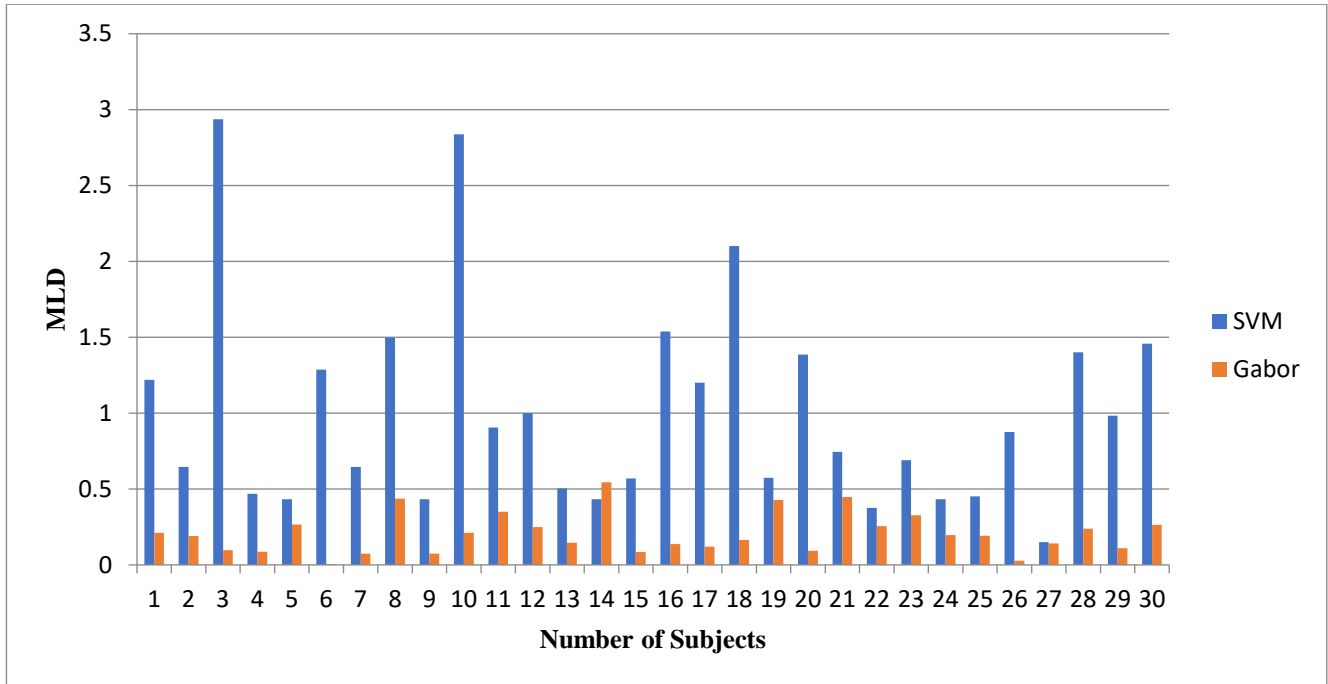


Fig. 6 Comparison of MLD of lumbar IVD localization by GFMM (n = 0.6mm) and SVM (n = 2mm)

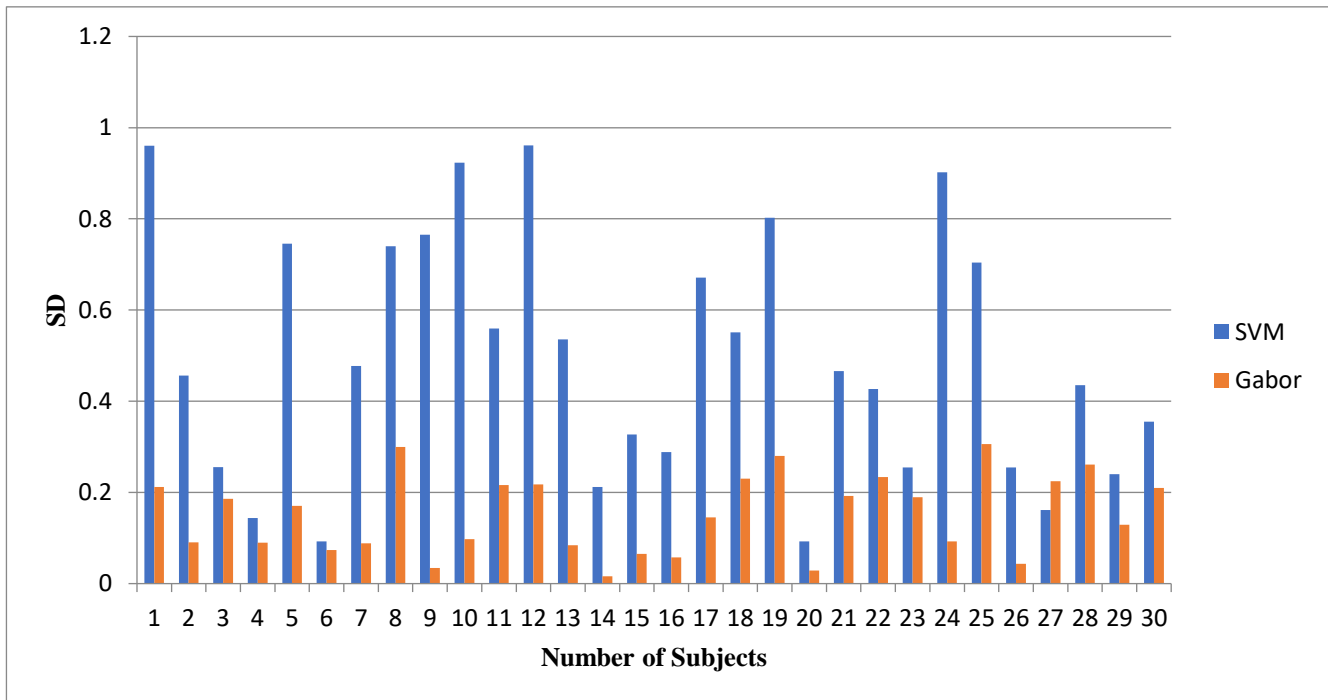


Fig. 7 Comparison of SD of lumbar IVD localization by GFMM (n = 0.6mm) and SVM (n = 2mm)

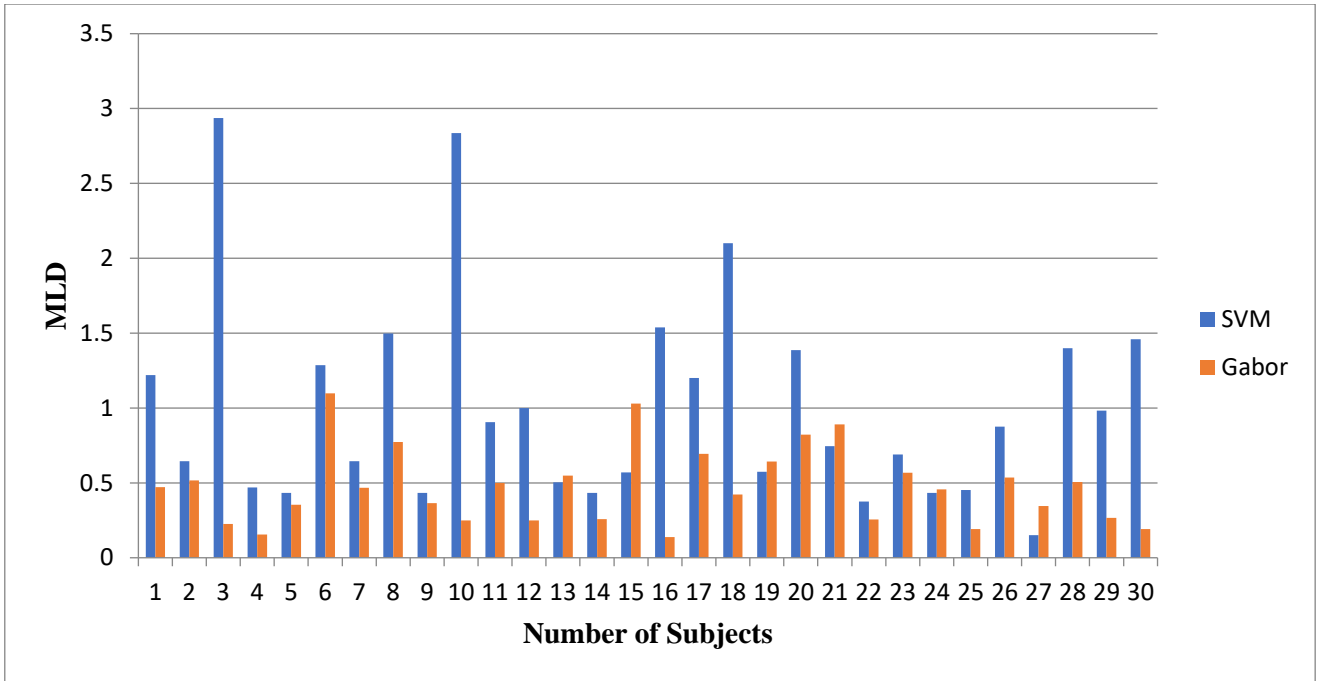


Fig. 8 Comparison of MLD of lumbar IVD localization by GFMM (n = 2mm) and SVM (n = 2mm)

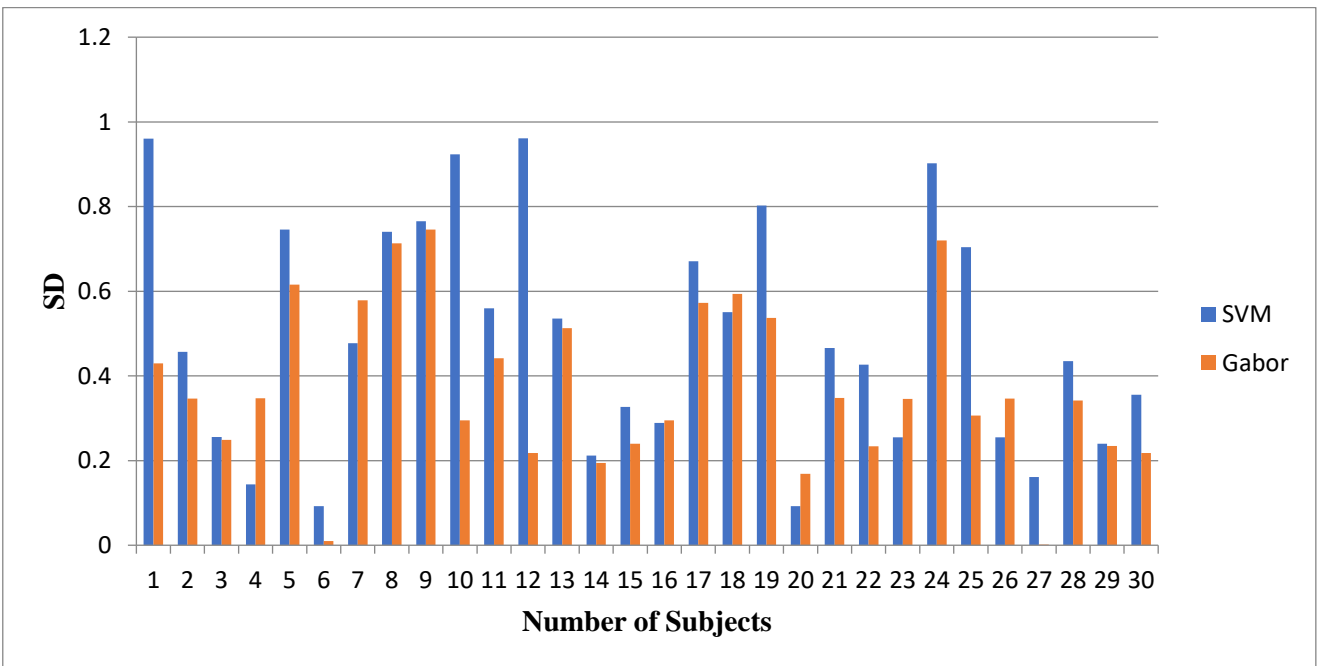


Fig. 9 Comparison of SD of lumbar IVD localization by GFMM (n = 2mm) and SVM (n = 2mm).

#### 4.7 Performance Analysis of Segmentation using Boundary Refined Region Growing Technique

The segmentation of lumbar IVD is done using a novel boundary refined region growing technique, and the evaluation of this segmentation performance was calculated using specificity, sensitivity, dice similarity index [6] is as follows:

$$\text{Specificity} = \frac{I - MUA}{I - M} \times 100\% \quad (9)$$

$$\text{Sensitivity} = \frac{M \cap A}{M} \times 100\% \quad (10)$$

$$\text{Dice Similarity Index} = \frac{2|M \cap A|}{|M| + |A|} \times 100\% \quad (11)$$

Where M is the manually segmented IVD area, A is the automatically segmented IVD area, and I is the MRI image. DSI measures the G and A similarity, and its values range from 0 to 100. Where '0' means no intersection and 100 means the complete intersection of G and A. the segmentation performance using the boundary refined region growing technique ranges from 98.5% to 99.6% specificity and 72.2% to 98.2% sensitivity. the overall average value for DSI, sensitivity, and specificity are

86.2%, 92%, and 99%, respectively; it also demonstrates a higher level of agreement between the proposed segmentation approach and manual segmentation.

## 5. Conclusion

The diagnosis of degeneration in lumbar IVD is done manually by a radiologist. It is a difficult and time-consuming technique that lacks repeatability across observers and depends on the radiologist's experience. The automated identification of IVD degeneration alleviates the significant strain on radiologists who must diagnose hundreds of patients every day using clinical MRI. This paper, automatic localization of lumbar IVD is done using the GFMM technique and SVM with LBP. Subsequently, the segmentation is done with a novel boundary refined region growing technique which makes the diagnosing

process easy for the radiologists. An MRI dataset of 180 IVDs from 30 patients validates the proposed technique. In comparing both the techniques, the accuracy of localization of GFMM is higher at 100% than the SVM with 89.4%. On the better accurate localized lumbar IVD image got by the GFMM technique, the segmentation is preceded by a novel boundary refined region growing technique achieving a DSI, sensitivity, and specificity of 86.2%, 92%, and 99%, respectively. The advantage of this work is that it does not need any manual intervention, and it gives a better localization and segmentation of lumbar IVDs. For the future scope of this work, the categories of degenerations in IVDs can be classified automatically with better accuracy.

## References

- [1] Modic, M.T, Ross., Lumbar Degenerative Disk Disease, *Radiology*, 245(1) (2007) 43-61.
- [2] An H.S., Introduction: Disc Degeneration: Summary. *Spine*, 29(23) (2004) 2677-2678.
- [3] Castro-Mateos I., 2D Segmentation of Intervertebral Discs and its Degree of Degeneration from T2-Weighted Magnetic Resonance Images, *SPIE Medical Imaging, International Society for Optics and Photonics*, (2014).
- [4] Michopoulou S.K., Atlas-Based Segmentation of Degenerated Lumbar Intervertebral Discs from M.R. Images of the Spine, *IEEE Transactions on Biomedical Engineering*, 56(9) (2019) 2225-2231.
- [5] Schmidt Et Al., Spine Detection and Labelling using A Parts-Based Graphical Model, *Biennial International Conference on Information Processing in Medical Imaging, Springer*, (2017).
- [6] Zhu X Et Al., A Method of Localization and Segmentation of Intervertebral Discs in Spine MRI Based on Gabor Filter Bank, *Biomedical Engineering Online*, 15(1) (2016).
- [7] Chevretils C Et Al., Watershed Segmentation of Intervertebral Disk and the Spinal Canal from MRI Images, *International Conference Image Analysis and Recognition, Springer*, (2007).
- [8] Oktay A.B. & Y.S. Akgul., Simultaneous Localization of Lumbar Vertebrae and Intervertebral Discs with SVM-Based MRF, *IEEE Transactions on Biomedical Engineering*, 60(9) (2013) 2375-2383.
- [9] Raja A, J.J. Corso & V. Chaudhary., Labelling Lumbar Discs using Both Pixel-and Object-Level Features with a Two-Level Probabilistic Model, *IEEE Transactions on Medical Imaging*, 30(1) (2011) 1-10.
- [10] Peng Z Et Al., Automated Vertebra Detection and Segmentation from the Whole Spine M.R. Images. in *Engineering in Medicine and Biology Society*, (2005).
- [11] Shi R Et Al., An Efficient Method for Segmentation of MRI Spine Images, *Complex Medical Engineering*, (2007).
- [12] Haq R Et Al., 3D Lumbar Spine Intervertebral Disc Segmentation and Compression Simulation From MRI using Shape-Aware Models, *International Journal of Computer-Assisted Radiology and Surgery*, 10(1) (2015) 45-54.
- [13] Vukadinovic D & M. Pantic., Fully Automatic Facial Feature Point Detection using Gabor Feature Based Boosted Classifiers. in *Systems, Man and Cybernetics*, (2005)
- [14] Kaya M & O. Bebek., Needle Localization using Gabor Filtering in 2D Ultrasound Images. in *Robotics and Automation (ICRA)*, (2014).
- [15] Hose J Et Al., Precise Localization of Landmarks on 3D Faces using Gabor Wavelets, *Biometrics: Theory, Applications, and Systems*, (2007).
- [16] Kumar A & G.K. Pang., Defect Detection in Textured Materials using Gabor Filters, *IEEE Transactions on Industry Applications*, 38(2) (2002) 425-440.
- [17] Oktay A.B. & Y.S. Akgul., Localization of the Lumbar Discs using Machine Learning and Exact Probabilistic Inference, *International Conference on Medical Image Computing and Computer-Assisted Intervention*, (2011).
- [18] Ghosh S Et Al., A New Approach to Automatic Disc Localization in Clinical Lumbar MRI: Combining Machine Learning with Heuristics. in *Biomedical Imaging (ISBI)*, (2012).
- [19] Kamarainen J.K., V. Kyrki, & H. Kalviainen. , Invariance Properties of Gabor Filter-Based Features-Overview and Applications, *IEEE Transactions on Image Processing*, 15(5) (2006) 1088-1099.
- [20] Lee T.S., Image Representation using 2D Gabor Wavelets, *IEEE Transactions on Pattern Analysis and Machine Intelligence*, 18(10) (1996) 959-971.
- [21] Daugman J.G., Complete Discrete 2-D Gabor Transforms by Neural Networks for Image Analysis and Compression, *IEEE Transactions on Acoustics, Speech, and Signal Processing*, 36(7) (1988) 1169-1179.
- [22] Haralick R.M, S.R. Sternberg & X. Zhuang., Image Analysis using Mathematical Morphology, *IEEE Transactions on Pattern Analysis and Machine Intelligence*, 4 (1987) 532-550.
- [23] Guo Z, L. Zhang & D. Zhang., Completed Modelling of Local Binary Pattern Operator for Texture Classification, *IEEE Transactions on Image Processing*, 19(6) (2010) 1657-1663.
- [24] Adankon M.M. & M. Cheriet., Support Vector Machine, *Encyclopedia of Biometrics*, (2009) 1303-1308.